HERBAL EXTRACT INHIBITION OF ZINC DOPED CALCIUM HYDROGEN PHOSPHATE DIHYDRATE CRYSTAL GROWTH AND PHYSICOCHEMICAL CHARACTERZATION

R.Selvaraju[*1]and M.Navaneetha[*2]

[*1]Engineering Physics, FEAT, Annamalai University, Annamalai Nagar, Tamilnadu, India

[*2] Department of Physics ,Annamalai University,Annamalai nager Tamilnadu

Abstract

The inhibitory effects of the medicinal plant extracts *Pedalium murex* and *Solanum xanthocarpum* were evaluated by growing different crystals such as Calcium hydrogen phosphate dihydrate (CHPD) and zinc-doped Calcium hydrogen phosphate dihydrate (Zn–CHPD) crystals using the single diffusion gel growth technique. The effect of different extract concentrations (0%, 5%, 10%, 15% and 20%) on the growth of crystals was systematically studied. Thermogravimetric and Differential Thermal analyses (TGA/DTA) were used to characterize the harvested crystals along with Fourier transform infrared (FTIR) spectroscopy, Fourier transform Raman (FT–Raman) spectroscopy and scanning electron microscopy (FESEM). From the thermal studies, it was observed that the thermal stability of CHPD crystals was enhanced by incorporation of zinc. FTIR and FT–Raman spectra revealed the characteristic functional groups of phosphates and hydroxyl groups, and showed some structural changes after the zinc doping. FESEM images revealed that the crystal morphology was changed by the incorporation of zinc, with higher aggregation and smaller crystal sizes than the undoped crystals. The results of crystal growth measurements showed that the crystal mass and crystal length decreased as the concentration of the extract increased. The extract of *Pedalium murex* was the most effective inhibitor and led to a significant decrease in the crystal size and yield compared with the other investigated extracts including that of *Solanum xanthocarpum*. The results indicate that the phytochemicals in the plant extracts are capable of inhibiting calcium phosphate crystal growth and could be considered as potential natural inhibitors to regulate the pathological mineralization process.

Keywords: **CHPD, Zn – CHPD, FESEM, FT – Raman, *Solanum xanthocarpum***

1 Introduction

The biomineralizations is a natural process where the inorganic minerals are deposited in biological systems under controlled physiological conditions. Calcium phosphate compounds are important biominerals and are abundant in bones, teeth and other calcified tissues [1]. Due to its significance in biological mineralization and biomaterials research and pathological calcification, calcium hydrogen phosphate dihydrate CHPD (brushite) has garnered much research interest among the different calcium phosphate phases [2]. CHPD is often found to be a precursor stage in the formation of other calcium phosphate minerals, and is commonly linked to urinary stone formation and abnormal mineralisation in biological tissues. Several factors affect the formation and growth of calcium phosphate crystals such as pH, supersaturation, ionic concentration, and presence of organic additives. Over the last few years many efforts have been devoted to the search for natural compounds that can be used to inhibit crystal nucleation and growth [3]. Plant-derived biomolecules are especially attractive as they are readily available, environmentally friendly and contain a variety of phytochemicals that can interact with the crystals surfaces. The naturally occurring compounds can affect the crystal growth by altering its surface energy, by inhibiting the attachment of ions and by changing the crystal morphology [4].

Traditional medicine has long used medicinal plants for the treatment of kidney stone related diseases. Of these, *Pedalium murex Solanum xanthocarpum* and are popular medicinal plants with a variety of curative properties. Both species have been used traditionally for diuretic, anti-inflammatory and anti- urolithiatic activities and the antioxidant, antimicrobial and therapeutic properties associated with the use of S. xanthocarpum for urinary tract disorders [5]. The phytochemical constituents present in the herbs such as flavonoids, alkaloids, phenolic compounds and saponins are thought to be of great importance in regulating crystal nucleation and aggregation of minerals. Apart from organic inhibitors, metal-ion doping has become a useful method to change the physicochemical properties of calcium phosphate materials. Zinc is an essential trace element with a variety of biological functions and known to affect mineralization behaviour. Zinc ions can be incorporated into calcium phosphate lattices and can alter the crystal growth kinetics, thermal stability, morphology and structural properties [6]. Thus, the system of the Zn doped calcium hydrogen phosphate dihydrate (Zn–CHPD) crystals is interesting for the study of the combined effect of the metal-ion substitution and of the natural growth inhibitors [7]. Gel growth technique is generally employed for the controlled growth of sparingly soluble crystals as the convection effect is reduced and it is an

ideal condition for slow crystal growth [8]. This technique allows investigation of crystal growth mechanism and the effect of different additives in a controlled environment. Zakrzewska et al. reported the synthesis and physicochemical characterization of Zn-doped brushite and demonstrated the successful incorporation of zinc into the brushite structure [9]. Chaima et al. investigated zinc-doped calcium phosphate sulfate hydroxyapatites and reported improved bioactivity, acceptable cytocompatibility, and enhanced antibacterial properties, indicating their suitability for biomedical applications [10].

In the present study the single diffusion gel technique has been used to grow CHPD and Zn–CHPD crystals in the presence of *Pedalium murex* extract and *Solanum xanthocarpum* extract at different concentrations. The inhibition effects of these herbal extracts on the crystal growth were investigated by measuring crystal mass and crystal length. In addition, the crystal growth was analysed by thermogravimetric and differential thermal analysis, Fourier transform infrared, Fourier transform Raman and scanning electron microscopy to reveal the structural, thermal and morphological changes upon the incorporation of zinc and plant extract treatment. The results gave useful information related to the use of medicinal plant extracts as natural inhibitors to control the calcium phosphate crystal growth and related pathological mineralization process.

2 Materials and Methods

2.1 Materials

Analytical grade sodium metasilicate ($Na_2SiO_3 \cdot 9H_2O$), zinc chloride ($Zncl_2$) and disodium hydrogen phosphate (Na_2HPO_4) were used to prepare the gel medium. Glacial acetic acid was employed to adjust the pH of the gel solution. All chemicals used in this study were of AnalaR grade and used without further purification.

2.2 Synthesis of CHPD crystal

Crystallization experiments were carried out using gel densities ranging from 1.03 to 1.06 g/cm³ and pH values between 4.0 and 6.5. The optimal conditions for brushite crystal formation were found to be a gel density of 1.03 g/cm³ and a pH of 6.0. After the gel had set, a calcium chloride solution was gently layered over it. Crystal nucleation began within approximately 24 hours, and small CHPD crystals were visibly formed within the gel matrix.

2.3 Preparation of leaf extract

The Fresh leaf (Pedalium Murex) ,solanum xanthocarbum were collected from B. Adhivaraga Nallur, Cuddalore District, Tamil Nadu, India. The collected flowers were thoroughly washed with distilled water to remove dust and other impurities. Subsequently, 80 g of the cleaned flowers were added to 400 mL of distilled water and heated until the volume was reduced to 100 mL. The resulting extract was filtered and stored under refrigerated conditions for further experimental studies. The prepared extract was used to investigate its inhibitory effect on brushite-type urinary crystals. Different concentrations of the extract were prepared as follows: 0% (control, distilled water only), 5% (5 mL extract + 15 mL distilled water), 10% (10 mL extract + 10 mL distilled water), 15% (15 mL extract + 5 mL distilled water), and 20% (20 mL extract only). These concentrations were subsequently employed for crystal growth inhibition studies. A similar procedure was followed for the preparation of extracts from other medicinal plants, namely pedalium murex. Solanum xanthocarpum. The extracts were prepared using the same extraction conditions and concentration ratios as described above.

2.4 Characterization

Fourier-transform infrared (FT-IR) spectra were recorded using a Shimadzu spectrometer in the range of 400–4000 cm^{-1}, employing a KBr beam splitter. Surface morphology was examined using a scanning electron microscope (FESEM, model S-300I). X-ray diffraction (XRD) analysis was performed using a PANalytical X'Pert PRO diffractometer. Thermal analysis (TG/DTA) was carried out using a NETZSCH STA 449F3 instrument to evaluate the thermal stability of the synthesized crystals.

3 Results and Discussion

3.1 Thermal Analysis

The thermal stability of the CHPD and Zn – CHPD crystals were examined by thermogravimetric analysis (TGA) and differential thermal analysis (DTA) as shown in Fig. 1(a) and Fig. 1(b) respectively. The TGA curve of the pure CHPD crystal (Fig. 1a) shows a continuous loss of weight with the temperature range studied. The initial reduction in mass is seen below 200 °C which is believed to be due to the loss of physically adsorbed water molecules and lattice bound water that is present in the crystal structure [11]. It is seen that weight loss is more noticeable in the range of 180-250 °C which corresponds to the dehydration of structural water of calcium hydrogen phosphate dihydrate. In the higher temperatures above this region, the crystal slowly and continuously loses mass up to 600 °C which corresponds to the progressive elimination of the volatile species remaining in the crystal and progressive rearrangement of the phosphate framework [12]. The total loss of weight at the end of the

analysis is in agreement with the moderate thermal stability of the CHPD crystal. From DTA curve of CHPD, a prominent endothermic peak around 200 °C is observed corresponding to the dehydration process and loss of water molecules from the crystal lattice.

A wide thermal event is observed at high temperature for which the transformation to a different structure and phase reorganization of the phosphate network are proposed. There are no sharp exothermic decomposition peaks which, in turn, indicates the absence of abrupt thermal degradation of the crystal in the range of the studied temperature. The thermal behaviour of the Zinc doped CHPD crystal (CHPDZ1) is presented in Fig. 1(b). Like undoped material, the first weight loss below 200 °C is associated with the removal of water molecules that are both adsorbed and coordinated to the surface. The doped crystal, however, shows a much lower dehydration rate, which is a characteristic of greater thermal stability to thermal decomposition. The decrease of mass in the range 250-500 °C might be associated with lattice rearrangement and stabilization of the phosphate structure in the presence of zinc ions. From 500 °C, weight is almost constant, indicating the stable formation of a thermal phase. The DTA profile of CHPDZ1 shows endothermic peaks around the dehydration region, and broad thermal transitions at higher temperatures. The shift of the thermal events and decrease of the rate of mass loss from the pure crystal suggest that the incorporation of zinc affects the crystal lattice and thus increases the thermal stability. The dopant ions can enhance bonding environment inside the phosphate structure which may retard the thermal degradation and create structural integrity during heating [13]. In general, the TGA/DTA curves showed that both crystal forms are highly thermally stable over a broad temperature range, and that zinc doping brings about increased thermal stability and better structural stability. The results indicate that the thermal properties of the crystals of calcium hydrogen phosphate dihydrate are improved with the incorporation of zinc ions and thus such crystals may be useful in applications requiring use at elevated temperatures.

3.2 FTIR analysis

The FTIR spectra of CHPD and Zn – CHPD crystals are presented in Fig. 2(a) and Fig. 2(b), respectively. The observed absorption bands confirm the presence of phosphate functional groups and water molecules within the crystal lattice For the pure CHPD crystal, characteristic absorption bands are observed at 537, 645, 792, 852, 997, 1138, 1182, 1231, 1684, 3270, 3438 and 3476 cm^{-1}. The bands appearing in the low-wavenumber region around 537 and 645 cm^{-1} are assigned to the bending vibrations of phosphate (PO_4^{3-}) groups [14]. The absorption peaks

located at 792 and 852 cm^{-1} correspond to P–O–H and phosphate-related vibrational modes [15]. The strong bands observed at 997, 1138, 1182 and 1231 cm^{-1} are attributed to the symmetric and asymmetric stretching vibrations of P–O bonds within the hydrogen phosphate framework [16]. The absorption band at 1684 cm^{-1} is associated with the bending vibration of water molecules present in the hydrated crystal structure. Broad absorption features centred around 3270–3476 cm^{-1} arise from O–H stretching vibrations, confirming the presence of lattice water and hydrogen-bonded hydroxyl groups [17].

The FTIR spectrum of the zinc-doped CHPD crystal exhibits absorption bands at 517, 615, 798, 868, 1155, 1182, 1653, 3176, 3347, 3452 and 3496 cm^{-1}. The bands detected below 700 cm^{-1} are related to phosphate bending vibrations and indicate that the fundamental phosphate framework remains intact after zinc incorporation. Peaks observed near 798 and 868 cm^{-1} are attributed to phosphate and hydrogen phosphate vibrational modes [18]. The strong absorption bands around 1155 and 1182 cm^{-1} correspond to P–O stretching vibrations of the phosphate groups. The band appearing at 1653 cm^{-1} is assigned to the bending mode of coordinated water molecules [19]. Furthermore, the broad absorption region between 3176 and 3496 cm^{-1} is associated with O–H stretching vibrations arising from water molecules and hydrogen-bond interactions within the crystal lattice [20]. A comparison of both spectra reveals slight shifts in several absorption bands after zinc incorporation. These shifts suggest an interaction between Zn^{2+} ions and the phosphate environment, leading to minor modifications in bond strength and local lattice symmetry. However, no new absorption bands corresponding to secondary phases are detected, indicating that zinc ions are incorporated into the CHPD lattice without altering the fundamental crystal structure. The preservation of the characteristic phosphate and hydroxyl vibrations confirms the successful formation of zinc-doped calcium hydrogen phosphate dihydrate crystals while maintaining the structural integrity of the host material. Overall, the FTIR results verify the presence of phosphate groups, structural water molecules and hydroxyl functionalities in both crystals. The observed band shifts in the doped sample provide evidence of zinc incorporation and its influence on the local bonding environment, while the retention of the major vibrational features demonstrates that the basic CHPD framework remains unchanged.

3.3 FT – Raman analysis

The CHPD and Zn – CHPD crystals Raman spectra are given in Fig. 3(a) and Fig. 3(b), respectively. The molecular vibrations and structural changes of zinc incorporation into the

CHPD lattice were studied using Raman spectroscopy. The Raman spectrum of the pure CHPD crystal shows strong bands around 566, 888, 1006, 1074 and 3276 cm-1. The strong band at 1006 cm-^{1} is attributed to the symmetric stretching of the phosphate (PO_4^{3-}) group, which is a typical band in calcium phosphate materials [21]. The Raman band near 1074 cm^{-1} is assigned to asymmetric P–O stretching vibrations, and the band at about 888 cm^{-1} is assigned to the hydrogen phosphate (HPO_4^{2-}) vibrations [22]. The low wave number band at 566 cm-1 is assigned to O–P–O bending vibrations of the phosphate tetrahedra. A wide band centered around 3276 cm^{-1} corresponds to the O–H stretching modes involving lattice water molecules and hydrogen bonds in the crystal lattice [23]. The characteristic bands of the Raman spectrum of the zinc doped CHPD crystal are at ~586, 898, 977, 1074 and 3358 cm^{-1}. As in the undoped crystal, the strong Raman band observed around 977 cm^{-1} is due to the symmetric stretching vibration of the phosphate groups. The symmetric and asymmetric P–O stretching vibrations are assigned to the peaks at 987 and 1074 cm^{-1}, respectively, which again show that the phosphate framework is retained after the incorporation of zinc. The band at 898 cm^{-1} is assigned to the vibrations of the hydrogen phosphate group, while the band at 586 cm^{-1} is from bending vibrations of the O–P–O group. The wide Raman band at 3358 cm–1 corresponds to the O–H stretching vibrations that occur in the crystal lattice when it is hydrated [24].

After comparing the spectra it can be noted that the positions of the Raman bands are slightly shifted after zinc doping. This is especially true of the stretching mode of the symmetric phosphate, which is observed at 1006 cm^{-1} for CHPD and 977 cm^{-1} for Zn - CHPD, suggesting changes in bonding environment that can be attributed to the presence of Zn^{2+} ions. The lattice distortion and the modification of the crystal field around the phosphate groups are further suggested by the similar variations in the low-frequency phosphate vibrations. Although these changes occurred, the dominant Raman bands of calcium hydrogen phosphate are still well discernible, thus indicating that the basic crystal structure is preserved after doping. No extra Raman bands are seen for secondary phases, suggesting that zinc ions are able to substitute into the CHPD lattice without the formation of detectable impurity compounds. The identified peak positions and intensities changes associated with the phosphate network validate the interaction between zinc ions and the phosphate network, which was found to cause a slight change in the structure while maintaining the crystal lattice framework. FT–Raman data overall indicate the successful growth of calcium hydrogen phosphate dihydrate crystals both pure and doped with zinc. Observed shifts in spectra and the retention of the characteristic phosphate vibrational

modes are indicative of the incorporation of the zinc and its effect on the local structure around the crystal lattice.

3.4 FESEM analysis

The surface morphology of CHPD and Zn – CHPD crystal were analyzed by scanning electron microscopy (FESEM) and the micrographs of the crystals are shown in Fig. 4(a) and Fig. 4(b), respectively. The FESEM image of pure CHPD crystal (Fig. 4a) shows that the crystalline particles formed are well developed and compact. The crystals are plate-like to block shaped with relatively smooth surfaces and crystal boundaries. The particles seem to be well crystallized and have uniform crystal growth during the synthesis. The texture of the surface is smooth and the facets are well-defined, indicating an orderly arrangement of ions in the crystal lattice [25]. Surface deposits that are observed on some crystal faces are minor and can be explained by secondary nucleation during crystal formation. The surface morphology of the zinc doped CHPD crystal is markedly different when compared to the FESEM micrograph of pure crystal as seen in Fig. 4b. The doped sample is made up of granular aggregates with irregular shapes and containing small crystallites. The particle size seems to be smaller and the surface is much rougher than that of the pure crystal, as there are many small grains present throughout the structure [26]. This coarsening of these microcrystalline particles results in a porous and heterogeneous surface structure. The morphologic changes detected showed an effect of the incorporation of Zn^{2+} ions on the nucleation and growth of CaHP crystals. The zinc ions could be interfering with the growth of larger crystal facets, causing the crystal to become smaller and have more irregularities in the surface. This behavior has been generally observed in lattice distortion and the change of lattice growth rate due to the incorporation of foreign ions into the host structure. Moreover, the decrease in the particle size and increase in surface roughness of the zinc doped sample can help to achieve a greater effective surface area. The modified surface properties could lead to better interactions between the material and its environment, such as in adsorption and ion exchange, bioactivity and catalytic processes. The overall FESEM investigation confirms that well-crystallized crystals of CHPD are formed, and that the morphology of the crystals becomes more compact with the addition of Zn doping, resulting in finer aggregated crystals with rougher crystal surfaces. These morphological changes confirm successful incorporation of zinc ions and reveal the effect of these ions on the crystal growth behaviour and microstructural properties of calcium hydrogen phosphate dihydrate crystals.

3.5 Crystal Growth Studies Using Plant Extracts

The effect of *Pedalium murex* & *Solanum xanthocarpum* extracts on the growth behaviour of pure and zinc doped calcium hydrogen phosphate dihydrate crystals was studied by varying the concentrations of the extracts (0%, 5%, 10%, 15% and 20%). The pictures of grown crystals are shown in Fig. 5 and Fig. 6. Figure 5 shows that crystals are grown with the help of extract of *Pedalium murex*. Without the extract (0%), the growth solution generated smaller, but more distinct crystals. Therefore, the crystal size and crystal yield decreased with increasing concentration of the extract (5% to 20%). Increased extract concentration led to increased turbidity of the solution, decreased crystal transparency, and smaller crystals. This behavior suggests that the phytochemical components contained in the extract have an interaction with the active growth part of the crystal surface, which inhibits normal crystal growth [27]. Organic molecules can be adsorbed on the crystal faces, which slow down incorporation of ions and inhibit growth of larger crystals.

The effect of *Solanum xanthocarpum* extract on the crystals grown was similar as illustrated in Fig. 6. The crystals in the control sample were well developed, while as the extract concentration was increased, a noticeable decrease was observed in the size of the crystal. The decrease in crystal growth, however, was somewhat less significant than the decrease in crystal growth in the case of the extract of *Pedalium murex*. The crystals at high concentration were smaller and more evenly distributed, indicating the extract components have a different effect on nucleation and crystal growth mechanisms. The presence of bioactive substances like alkaloids, flavonoids and phenolics may change the supersaturation conditions and may disrupt the orderly positioning of ions in the crystal lattice [28]. There is a decrease in crystal size with the increase in concentration of extracts, indicating that both plant extracts have an effect as crystal growth modifier. A crystal growth inhibition effect of these additives can be achieved by adsorption on energetically favourable crystal faces, which results in a decrease in crystal growth rates and inhibits the growth of larger crystals. This ability to inhibit is useful in research involving pathological biomineralization as the formation of large mineral deposits is undesirable, so controlling growth is desired.

The comparison of the two extracts shows that extract of *P. murex* has a greater crystal growth inhibitory effect than *S. xanthocarpum*. The observed decrease of crystal size indicates the greater affinity of the phytoconstituents of *P. murex* towards the crystal surface, which is further explained by the decrease of crystal mass observed in the treated samples. This

increased inhibitory effect could be explained by the presence of higher amounts of functional groups that could interact with calcium and phosphate ions during the crystal formation. It is concluded that the overall observations of the photographs agree that the crystal growth is progressively reduced with an increase in concentration of the extract. The results proved that both plant extracts exhibited the ability to inhibit the crystal growth to a good extent, and *Pedalium murex* exhibited comparatively higher ability to inhibit the crystal growth under the same experimental conditions.

3.6 Crystal Growth Inhibition Studies

The harvested CHPD and Zn – CHPD crystals in the presence of various concentrations of the extracts of Pedalium murex and Solanum xanthocarpum are presented in the following figures. 7–10. The photos depict directly the effect of plant extract on the crystal growth, crystal morphology and the crystal yield. The crystals formed with extract of Pedalium murex were comparatively large and well-developed with comparatively low concentration (0%) (Fig. 7). The crystal size decreased with increasing concentration of the extract (from 5% to 20%). As the concentration of the extract increased, the thickness, length and number of crystals decreased. Only small fragmented crystals were obtained at 20% concentration of extract, showing that there was significant suppression of crystal growth. This behaviour indicates that the bioactive parts of the extract attach to the growing faces of the crystal and inhibit crystal growth rates.

The same trend was noticed for the Zn–CHPD crystals formed in the presence of Pedalium murex extract (Fig. 8). The crystals collected demonstrated a decreasing size pattern with increasing concentration of extract. At higher concentrations however, the morphology of the crystals was irregular and there was more fragmentation compared to the pure CHPD crystals. This observation suggests that the combined effect of Zn incorporation and the adsorption of phytochemicals changes the crystal growth process and prevents the growth of larger crystals. The harvest crystals of CHPD and Zn–CHPD are shown in Figures 9 and 10 respectively with the help of extract of *Solanum xanthocarpum*. The control samples yielded elongated plate like crystals, having relatively larger dimensions. As the concentration of the extract increased, the size of the crystals started to decrease gradually and the quantity of smaller crystals increased. The crystals were still seen to inhibit growth, but the crystals' characteristic morphology was seen over a wider range of concentrations compared to the *Pedalium murex* treated samples. From this result, it has been suggested that the inhibitory

effect of the plant *Solanum xanthocarpum* is less intense as compared to other plants. The length of the crystals observed with the eye also confirms the measurements. Both plant extract inhibited crystal growth in a concentration dependent manner. The effect of phytochemicals like flavonoids, phenolic compounds, alkaloids and other oxygen containing functional groups with calcium and phosphate ions present in the growth media may be responsible for the reduction in crystal size. These do not only influence the nucleation kinetics but also can block energetically favourable faces of crystal growth, suppressing crystal enlargement.From the comparison of both extracts, it can be said that the crystal growth inhibiting properties of Pedalium murex is greater than that of Solanum xanthocarpum. The higher the concentration of the *Pedalium murex*, the smaller and more fragmented the crystals. The increased inhibitory effect might be due to the increased affinity of the phytoconstituents to the surface of the crystals and to the ionic species in solution. The overall crystal images obtained after harvesting clearly indicate that both the plant extracts have an effect on the growth behaviour of crystals of CHPD and Zn–CHPD. As the concentration of the extracts increased, the crystal size got smaller and the crystal yield became lesser, which proved the effectiveness of the extracts as natural crystal growth inhibitors. Of the extracts studied, Pedalium murex exhibited the highest inhibitory activity, strongly inhibiting the crystal growth at 15% and 20% extract concentrations.

3.7 Effect of Herbal Extracts on Crystal Mass

The effect of *Pedalium murex* and *Solanum xanthocarpum* extracts on the mass of CHPD and Zn – CHPD crystals is presented in Fig. 11(a) and Fig. 11(b), respectively. Crystal mass is an important parameter for evaluating the extent of crystal growth and the inhibitory action of additives present in the growth medium. For the CHPD crystals (Fig. 11a), the control sample without extract exhibited the highest crystal mass of 0.864 mg. Upon the addition of *Pedalium murex* extract, the crystal mass decreased progressively from 0.348 mg at 5% concentration to 0.034 mg at 20% concentration. Similarly, in the presence of *Solanum xanthocarpum* extract, the crystal mass decreased from 0.365 mg at 5% concentration to 0.048 mg at 20% concentration. The gradual decline in crystal mass with increasing extract concentration indicates that both herbal extracts effectively suppress crystal growth. The reduction was particularly pronounced at concentrations above 10%, where a substantial decrease in crystal yield was observed.

A similar trend was obtained for the Zn–CHPD crystals (Fig. 11b). The control crystal showed a mass of 1.123 mg, which was higher than that of the undoped CHPD crystal, indicating enhanced crystal growth in the presence of zinc ions. However, the addition of plant extracts significantly reduced crystal mass. In the case of *Pedalium murex*, the mass decreased from 0.668 mg at 5% concentration to 0.085 mg at 20% concentration. Likewise, *Solanum xanthocarpum* reduced the crystal mass from 0.675 mg at 5% concentration to 0.081 mg at 20% concentration. These results confirm that increasing extract concentration progressively inhibits the accumulation of crystal material during growth. The observed reduction in crystal mass can be attributed to the adsorption of phytochemical constituents on active crystal growth sites. Bioactive compounds such as flavonoids, phenolics, alkaloids and other organic molecules present in the extracts may interact with calcium and phosphate ions, thereby reducing ion availability and restricting crystal growth [29]. Such interactions can alter nucleation and growth kinetics, resulting in smaller crystals and lower crystal yield. Comparison of the two extracts shows that *Pedalium murex* exhibited slightly greater inhibition toward CHPD crystal growth, particularly at higher concentrations where the lowest crystal mass was recorded. For Zn–CHPD crystals, both extracts produced comparable inhibitory effects, although minor variations were observed at individual concentrations. The overall reduction in crystal mass demonstrates the effectiveness of the plant extracts as crystal growth modifiers. The inhibitory efficiency increased with extract concentration, indicating a concentration-dependent response. This behaviour suggests that the active phytochemicals become more effective as their concentration in the growth medium increases, leading to stronger interactions with the crystal surface and greater suppression of crystal development [30]. Overall, the crystal mass measurements clearly demonstrate that both *Pedalium murex* and *Solanum xanthocarpum* extracts significantly reduce the growth of CHPD and Zn–CHPD crystals. The results support the potential application of these herbal extracts as natural inhibitors of calcium phosphate crystal formation and growth.

3.8 Effect of Herbal Extracts on Crystal Length

The influence of *Pedalium murex* and *Solanum xanthocarpum* extracts on the length of CHPD and Zn – CHPD crystals is illustrated in Fig. 12(a) and Fig. 12(b), respectively. Crystal length serves as an important indicator for assessing the extent of crystal growth and the effectiveness of growth-inhibiting agents. For the CHPD crystals (Fig. 12a), the control sample exhibited the maximum crystal length of 30 mm. The addition of herbal extracts resulted in a

marked reduction in crystal size. In the presence of *Pedalium murex*, the crystal length decreased from 11 mm at 5% concentration to 2 mm at 20% concentration. A similar trend was observed with *Solanum xanthocarpum*, where the crystal length decreased from 11 mm at 5% concentration to 3 mm at 20% concentration. The sharp decline in crystal length demonstrates that both extracts effectively restrict crystal growth, with the inhibition becoming more pronounced as the extract concentration increases [31]. The Zn–CHPD crystals (Fig. 12b) also exhibited a concentration-dependent reduction in crystal length. The control crystal attained a length of 16 mm, whereas the addition of *Pedalium murex* reduced the length to 10, 8, 6 and 3 mm at concentrations of 5%, 10%, 15% and 20%, respectively. In the case of *Solanum xanthocarpum*, the crystal lengths were 11, 9, 8 and 4 mm for the corresponding concentrations. Although crystal growth was inhibited in both cases, the reduction was comparatively less severe than that observed for the undoped CHPD crystals, suggesting that zinc incorporation influences crystal growth behaviour and modifies the response to the plant extracts. The decrease in crystal length with increasing extract concentration can be attributed to the adsorption of phytochemical constituents onto active crystal growth faces. Compounds such as phenolics, flavonoids, alkaloids and other organic molecules present in the extracts may interact with calcium and phosphate ions in solution or bind to specific crystal planes, thereby reducing the rate of ion deposition and crystal elongation [32]. As a result, crystal growth becomes progressively restricted, leading to shorter crystals.

A comparison of the two extracts indicates that *Pedalium murex* generally produced a greater reduction in crystal length than *Solanum xanthocarpum*. For CHPD crystals, the crystal length decreased by approximately 93% at 20% concentration of *Pedalium murex*, whereas the reduction was about 90% for *Solanum xanthocarpum*. A similar trend was observed in the Zn–CHPD system, where *Pedalium murex* consistently yielded smaller crystals at equivalent concentrations. These observations suggest that the active phytoconstituents of *Pedalium murex* possess a stronger affinity for the crystal surface and exhibit greater crystal growth inhibition. The results clearly demonstrate a concentration-dependent inhibitory effect of both herbal extracts on crystal growth. Increasing extract concentration significantly suppresses crystal elongation, indicating that the extracts interfere with the normal growth mechanism of calcium hydrogen phosphate crystals. Such inhibition is of particular interest in studies related to biomineralization control, where reducing crystal size is essential for preventing excessive crystal aggregation and deposition. Overall, the crystal length measurements confirm that both *Pedalium murex* and *Solanum xanthocarpum* act as effective natural crystal growth inhibitors.

Among the two extracts, *Pedalium murex* exhibited a comparatively stronger inhibitory effect on both CHPD and Zn–CHPD crystals, particularly at higher concentrations, where the smallest crystal dimensions were obtained.

4 Conclusion

The Pure calcium hydrogen phosphate dihydrate and zinc doped calcium hydrogen phosphate dihydrate crystals were successfully grown by gel diffusion method and growth behaviour of these crystals was studied in the presence of *Pedalium murex* and *Solanum xanthocarpum* extract. Thermal analysis showed that the enhancement of thermal stability of the host crystal by zinc incorporation was confirmed. The FTIR and FT–Raman studies confirmed the preservation of the phosphate framework and the small change in the spectra due to the introduction of the zinc atoms. The FESEM analysis showed major changes in the crystals morphology with doping, such as a decrease in particle size and increase in surface irregularity. The crystal growth inhibition studies demonstrated that both herbal extracts were able to inhibit crystal growth in a concentration-dependent manner, with both the crystal mass and crystal length being inhibited. The crystal growth was progressively suppressed with the increase of concentration of the extract, which shows strong interaction of the phytochemical constituents with the active crystal growth sites. *Pedalium murex* exhibited relatively higher inhibitory activity than *Solanum xanthocarpum* especially at higher concentrations. The decrease in the crystal size and reduction in crystal yield indicates that the extracts affect the nucleation and crystal growth mechanism, possibly through modification of the ion mobility and surface growth mechanism. In overall, the present study shows that the extracts of *Pedalium murex* and *Solanum xanthocarpum* are effective natural crystal growth inhibitors. The findings have implications for their use in the prevention of calcium phosphate crystal formation in plants and will prove useful in designing plant based strategies to prevent pathological biomineralization and associated crystal deposition problems.

References

1. Dorozhkin, S. V., & Epple, M. (2002). Biological and medical significance of calcium phosphates. Angewandte Chemie International Edition, 41(17), 3130-3146.
2. Eliaz, N., & Metoki, N. (2017). Calcium phosphate bioceramics: a review of their history, structure, properties, coating technologies and biomedical applications. Materials, 10(4), 334.

3. Zhang, Y., Li, B., Liu, J., Han, D., Rohani, S., Gao, Z., & Gong, J. (2024). Inhibition of crystal nucleation and growth: a review. Crystal Growth & Design, 24(6), 2645-2665.
4. Salzmann, B. B., Van Der Sluijs, M. M., Soligno, G., & Vanmaekelbergh, D. (2021). Oriented attachment: from natural crystal growth to a materials engineering tool. Accounts of chemical research, 54(4), 787-797.
5. Patel, P. K., Patel, M. A., Vyas, B. A., Shah, D. R., & Gandhi, T. R. (2012). Antiurolithiatic activity of saponin rich fraction from the fruits of Solanum xanthocarpum Schrad. & Wendl.(Solanaceae) against ethylene glycol induced urolithiasis in rats. Journal of ethnopharmacology,
6. Kumar, P. N., Ponnilavan, V., Lee, W., & Yoon, J. (2022). Zinc additions in calcium phosphate system. Phase behavior, microstructural and mechanical compatibility during sequential heat treatments. Journal of Alloys and Compounds, 929, 167173. 144(1), 160-170.
7. Kareem, R. O., Barzinjy, A. A., Ates, T., Bulut, N., Keser, S., & Kaygili, O. (2025). Advances in metallic ion-doped hydroxyapatite: unlocking enhanced structural, biological, and functional properties for cutting-edge biomedical applications. Journal of the Australian Ceramic Society, 1-33.
8. Velásquez-González, O., Campos-Escamilla, C., Flores-Ibarra, A., Esturau-Escofet, N., Arreguin-Espinosa, R., Stojanoff, V & Moreno, A. (2019). Crystal growth in gels from the mechanisms of crystal growth to control of polymorphism: new trends on theoretical and experimental aspects. Crystals, 9(9), 443.
9. Laskus-Zakrzewska, A., Zgadzaj, A., & Kolmas, J. (2021). Synthesis and physicochemical characterization of Zn-doped brushite. Ceramics International, 47(6), 7798-7804.
10. Wacharine, C., Dridi, A., Hassen, S. B., Nouri, F., Mosbah, A., Charradi, K., ... & Ternane, R. (2024). Zinc doped calcium phosphate-sulfate hydroxyapatites: Synthesis, characterization, bioactivity, cytotoxicity and antibacterial properties. Ceramics International, 50(22), 44773-44784.
11. Srinivasan, S. G., Shivaramaiah, R., Kent, P. R., Stack, A. G., Navrotsky, A., Riman, R., ... & Bryantsev, V. S. (2016). Crystal structures, surface stability, and water adsorption energies of La-bastnäsite via density functional theory and experimental studies. The Journal of Physical Chemistry C, 120(30), 16767-16781.
12. Wang, X., Wu, T., Hong, J., Dai, J., Lu, Z., Yang, C., ... & Dai, L. (2021). Organophosphorus modified hollow bimetallic organic frameworks: Effective adsorption and catalytic charring of pyrolytic volatiles. Chemical Engineering Journal, 421, 129697.
13. Li, H., Yi, J., Qin, Z., Sun, Z., Xu, Y., Wang, C., ... & Liang, X. (2019). Structures, thermal expansion, chemical stability and crystallization behavior of phosphate-based glasses by influence of rare earth. Journal of Non-Crystalline Solids, 522, 119602.
14. Frost, R. L., Xi, Y., Scholz, R., López, A., Lima, R. M. F., & Ferreira, C. M. (2013). Vibrational spectroscopic characterization of the phosphate mineral series eosphorite–childrenite–(Mn, Fe) Al (PO4)(OH) 2·(H2O). Vibrational Spectroscopy, 67, 14-21.
15. Chen, H., Li, M., Zhong, Z., Seim, I., Wang, M., Lian, C., ... & Li, C. (2025). Function and Development of Deep-sea Mussel Bacteriocytes Revealed by SnRNA-seq and Spatial Transcriptomics. Genomics, Proteomics & Bioinformatics, qzaf109.

16. Rafik, A., Lakhdar, F., Zouihri, H., Guedira, T., Acharjee, N., Islam, M. S., ... & Zeroual, A. (2024). Exploring nonlinear optical properties in a hybrid dihydrogen phosphate system: an experimental and theoretical approach. Journal of Molecular Modeling, 30(5), 151.
17. Azeez, S., & Shenbagaraman, R. (2025). Fourier transform infrared spectroscopy in characterization of bionanocomposites. In Characterization Techniques in Bionanocomposit
18. Trivedi, M. K., Branton, A., Trivedi, D., Nayak, G., Bairwa, K., & Jana, S. (2015). Spectroscopic characterization of disodium hydrogen orthophosphate and sodium nitrate after biofield treatment. Journal of Chromatography & Separation Techniques, 6(5). es (pp. 209-227). Woodhead Publishing.
19. Han, L., Sun, Y., Cai, W., & Shao, X. (2023). Seeking the structure of water from the combination of bending and stretching vibrations in near infrared spectra. Journal of Near Infrared Spectroscopy, 31(4), 204-210.
20. Ghosh, N., Bandyopadhyay, A., Roy, S., Saha, G., & Mondal, J. A. (2023). Unified view of the hydrogen-bond structure of water in the hydration shell of metal ions (Li+, Mg2+, La3+, Dy3+) as observed in the entire 100–3800 cm− 1 regions. Journal of Molecular Liquids, 389, 122927.
21. Ramaiah, G., Meko, R. L., Abreham, A., Negawo, T. A., Baraki, S. Y., & Asfaw, D. (2026). Development of eco-friendly, flame-retardant cotton fabric via coating with calcium phosphate extracted from waste chicken bones. Journal of Material Cycles and Waste Management, 28(1), 232-252.
22. Syed, K. A., Pang, S. F., Zhang, Y., Zeng, G., & Zhang, Y. H. (2012). Micro-Raman observation on the HPO42–association structures in an individual dipotassium hydrogen phosphate (K2HPO4) droplet. The Journal of Physical Chemistry A, 116(6), 1558-1564.
23. Ram, S. (2001). Infrared spectral study of molecular vibrations in amorphous, nanocrystalline and AlO (OH)· αH2O bulk crystals. Infrared physics & technology, 42(6), 547-560.
24. Piszczek, P., Grodzicki, A., & Engelen, B. (2003). Infrared and Raman studies of water molecule normal vibrations in crystalline hydrates which form the chain structures. Journal of Molecular Structure, 646(1-3), 45-54.
25. Jiang, Z. Y., Kuang, Q., Xie, Z. X., & Zheng, L. S. (2010). Syntheses and properties of micro/nanostructured crystallites with high-energy surfaces. Advanced Functional Materials, 20(21), 3634-3645.
26. Wouters, O., Vellinga, W. P., van Tijum, R., & De Hosson, J. T. M. (2006). Effects of crystal structure and grain orientation on the roughness of deformed polycrystalline metals. Acta Materialia, 54(10), 2813-2821.
27. Jothibas, M., Paulson, E., Srinivasan, S., & Kumar, B. A. (2022). The impacts of interfacing phytochemicals on the structural, optical and morphology of hematite nanoparticles. Surfaces and Interfaces, 29, 101734.
28. Rathi, R., Kaur, S., & Singh, I. (2022). A review on co-crystals of herbal bioactives for solubility enhancement: preparation methods and characterization techniques. Crystal Growth & Design, 22(3), 2023-2042.
29. Makbul, S. A. A., Jahan, N., & Kalam, M. A. (2019). Bio-active compounds from unani medicinal plants and their application in urolithiasis. In Natural Bio-active Compounds:

Volume 2: Chemistry, Pharmacology and Health Care Practices (pp. 369-407). Singapore: Springer Singapore.

30. Kaur, H., Kumar, S., & Bouzid, G. (2024). Exploring the role of different phytochemicals on the morphological variations of metal and metal oxide nanomaterials for biomedical application. Interactions, 245(1), 234.
31. Chauhan, C. K., Joshi, M. J., & Vaidya, A. D. B. (2009). Growth inhibition of struvite crystals in the presence of herbal extract Commiphora wightii. Journal of Materials Science: Materials in Medicine, 20(Suppl 1), 85-92.
32. Menon, S., Shinisha, C. B., Al Mamari, H. K., Al Zaabi, H. H., Al Ajmi, Z. S., Al-Jaradi, A. Z. H., ... & Jayachandran, V. P. (2024). Experimental and theoretical studies on the modulation of the crystallization process and crystal morphology of calcium oxalate using Moringa oleifera bark extract. Journal of Molecular Structure, 1305, 137693.

Figure ;

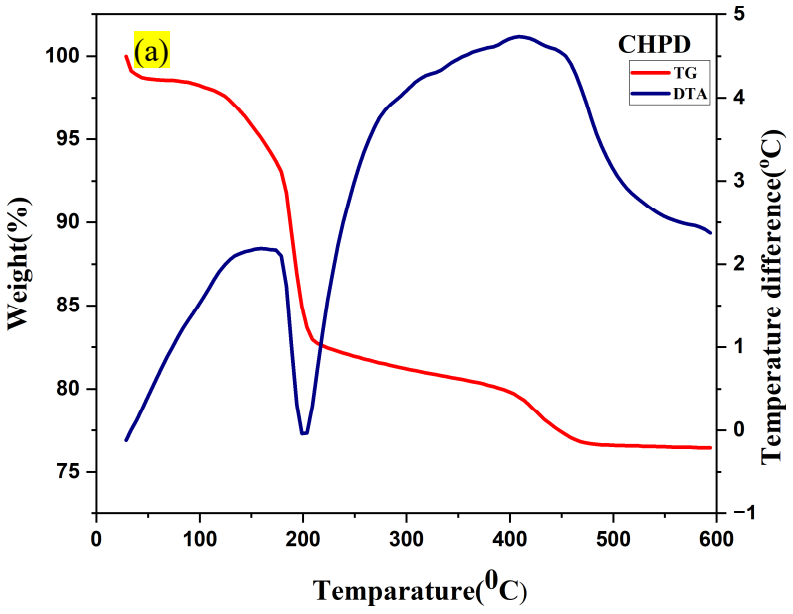

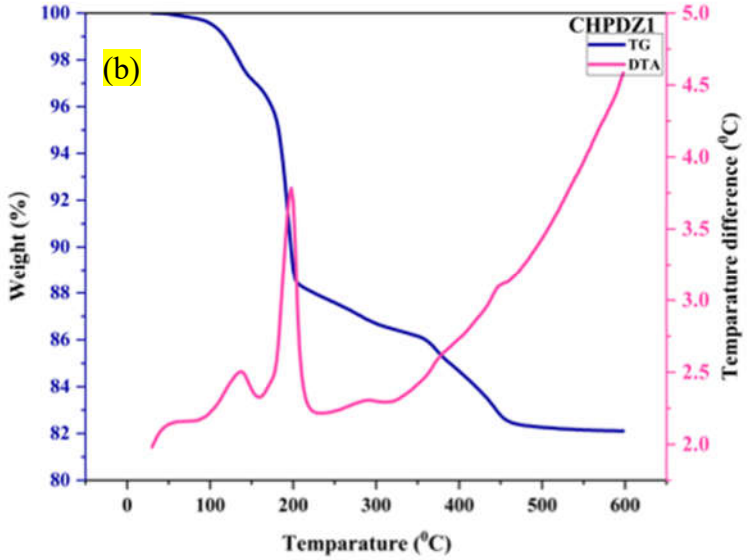

Figure 1 TGA/DTA spectrum of (a) CHPD and (b) Zn – CHPD crystal

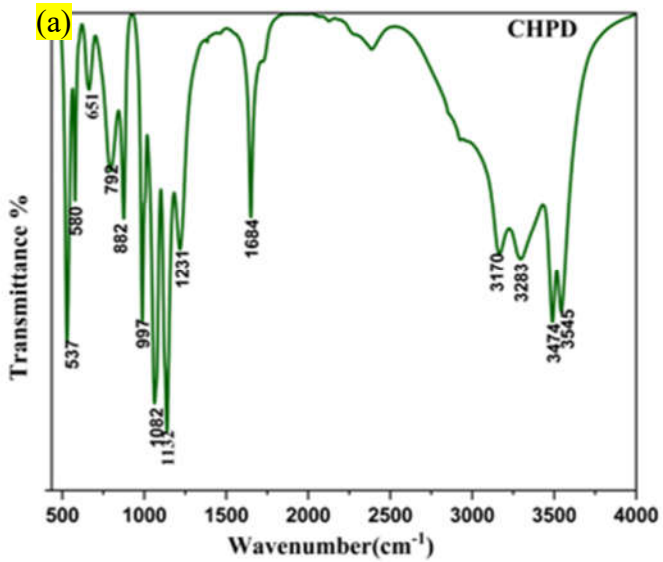

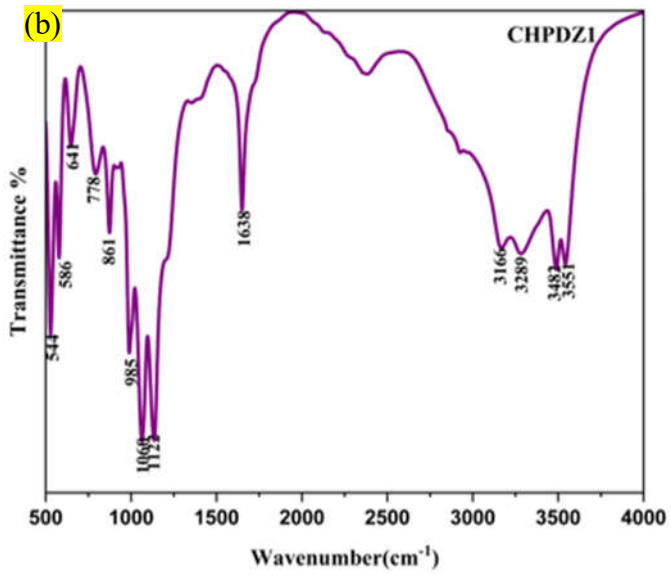

Figure 2 FTIR spectrum of (a) CHPD and (b) Zn – CHPD crystal

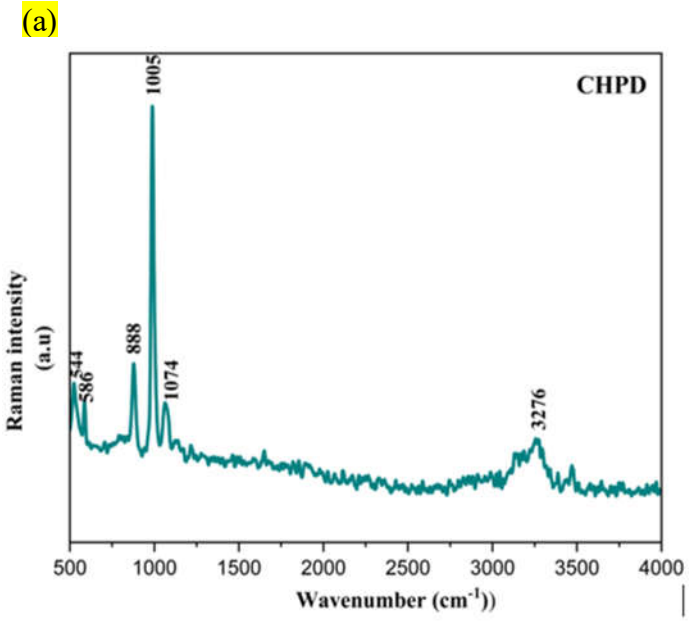

(b)

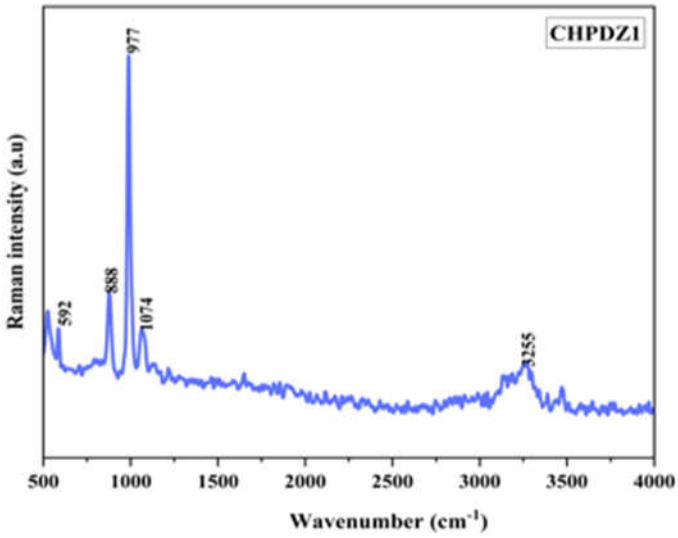

Figure 3 FT – Raman spectrum of (a) CHPD and (b) Zn – CHPD crystal

(a)

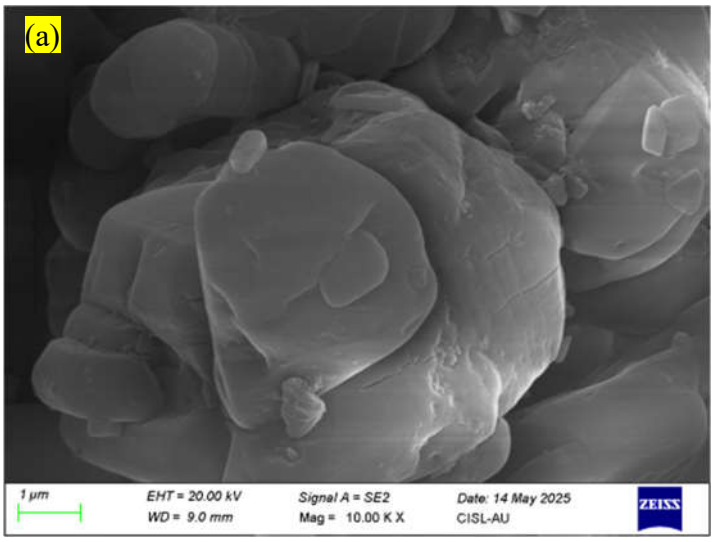

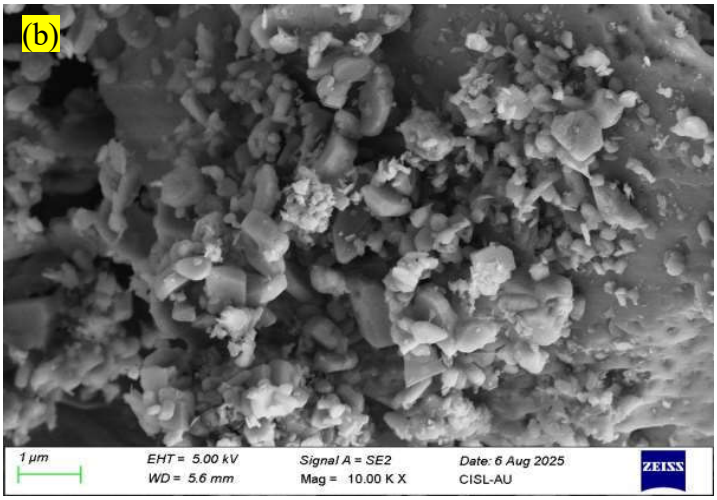

Figure 4 FESEM image of spectrum of (a) CHPD and (b) Zn – CHPD crystal

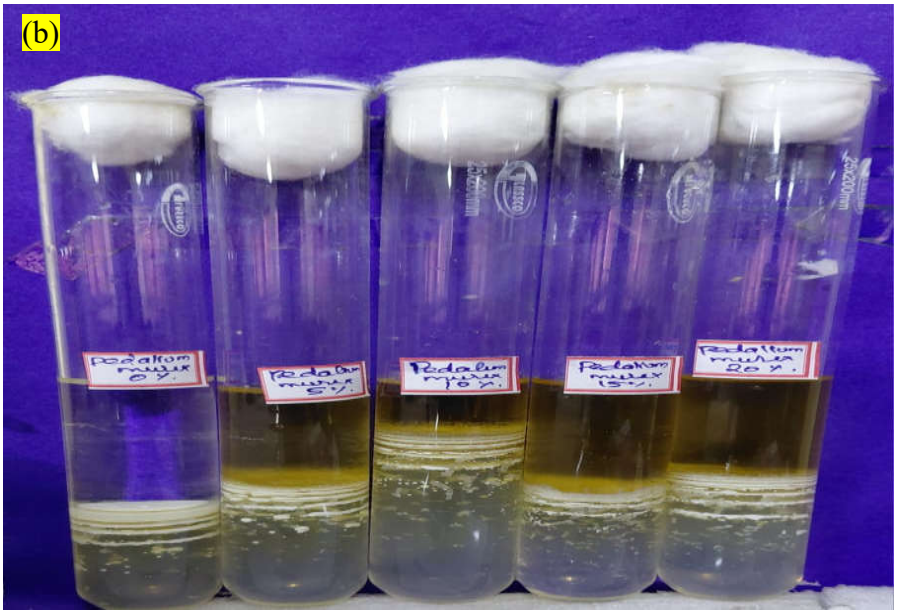

Figure 5 Photograph image of **(a) CHPD and (b) Zn – CHPD crystal** crystal different concentration of *Pedalium murex* extract (0%, 5%, 10%, 15%, and 20%)

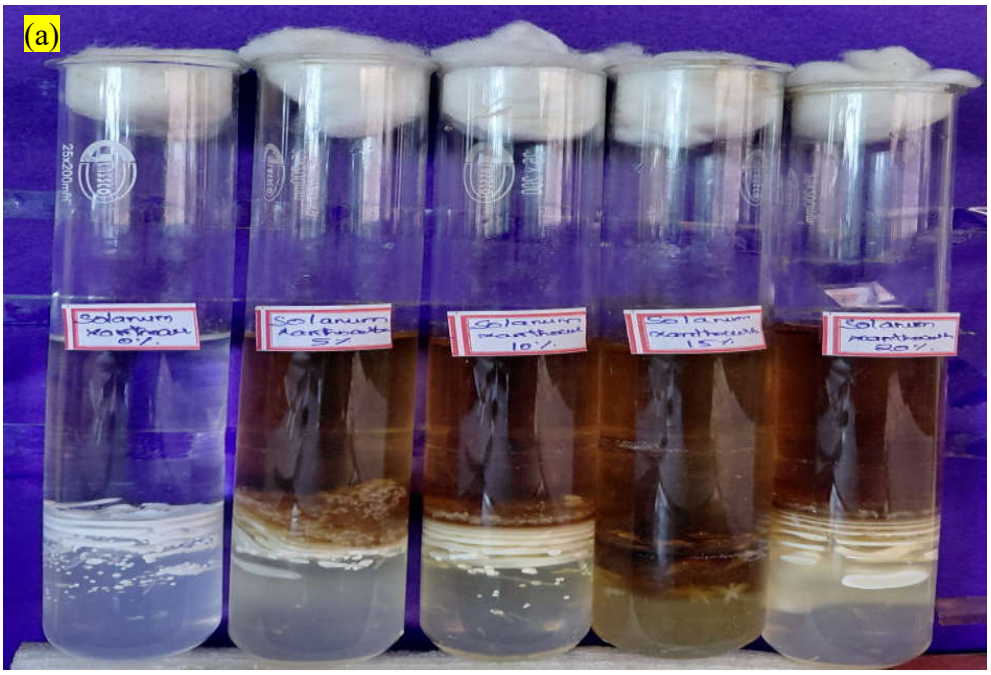

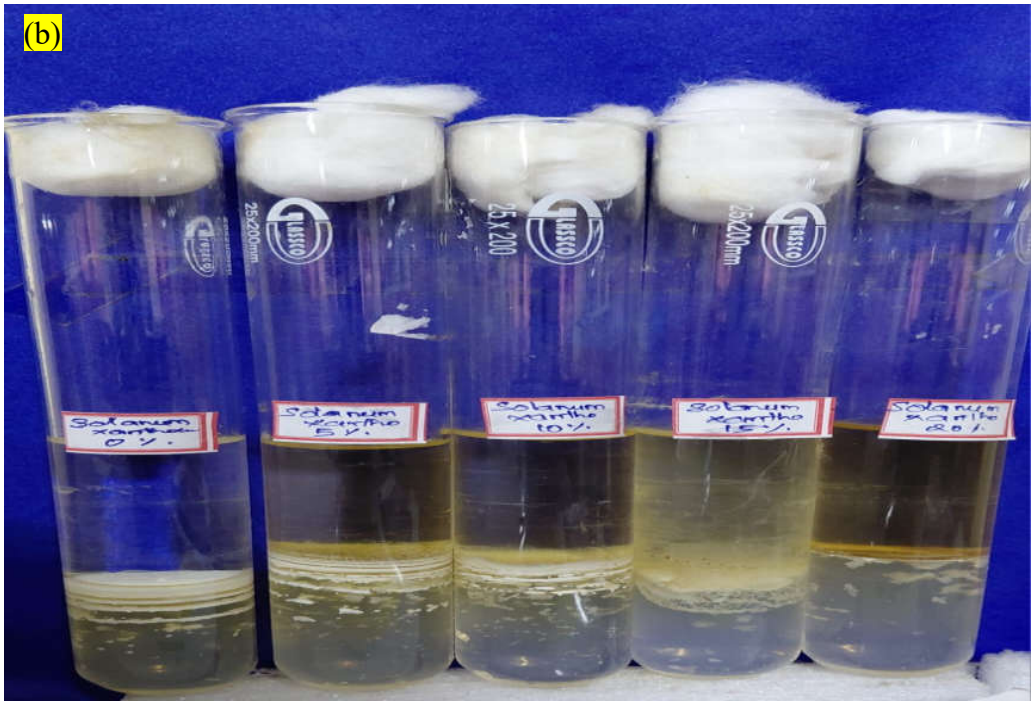

Figure 6 Photograph image of **(a) CHPD and (b) Zn – CHPD crystal** crystal different concentration of *Solanum xanthocurbum* extract (0%, 5%, 10%, 15%, and 20%)

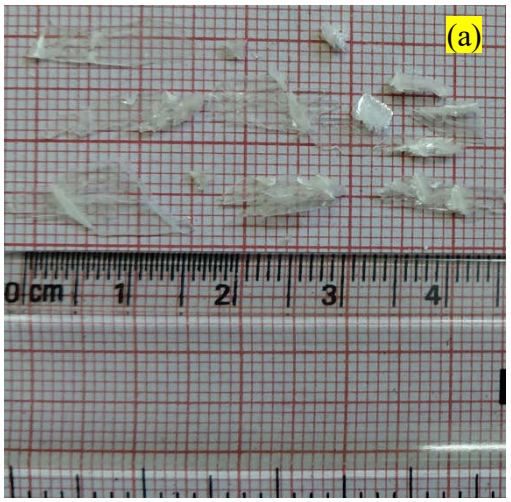

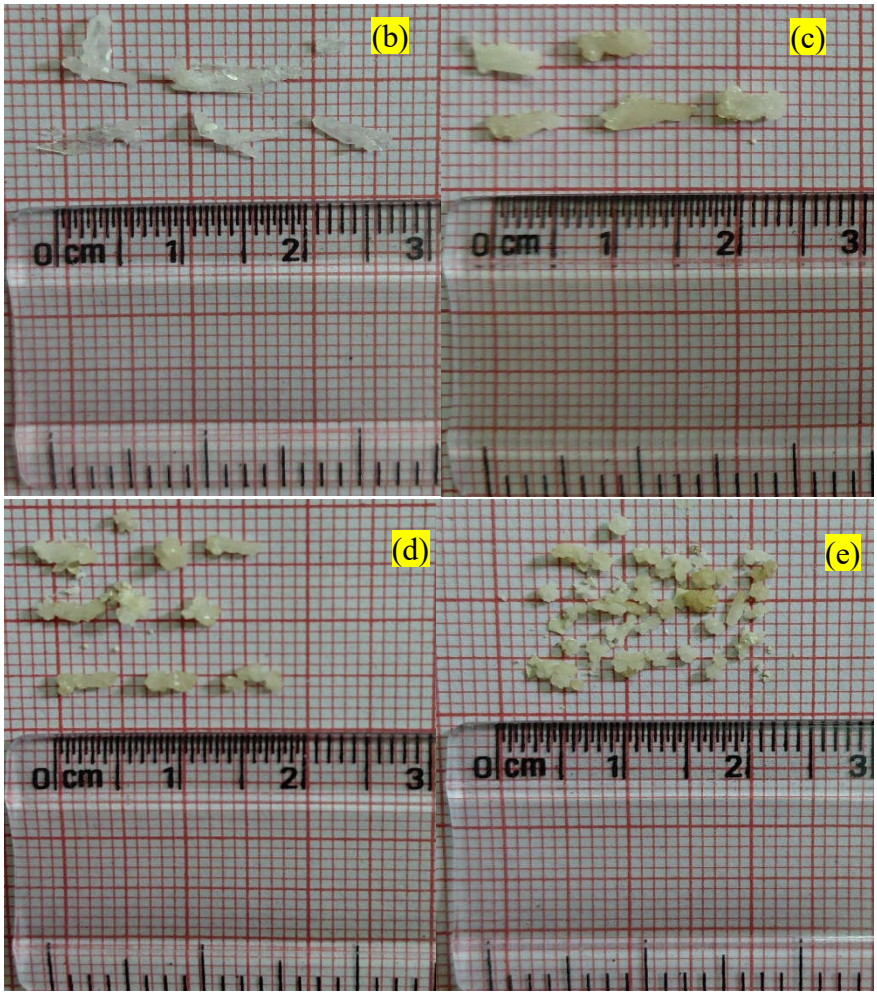

Figure 7 Fig. 7. Harvested CHPD crystals grown in the presence of different concentrations of Pedalium murex extract: (a) 0%, (b) 5%, (c) 10%, (d) 15% and (e) 20%.

(a)

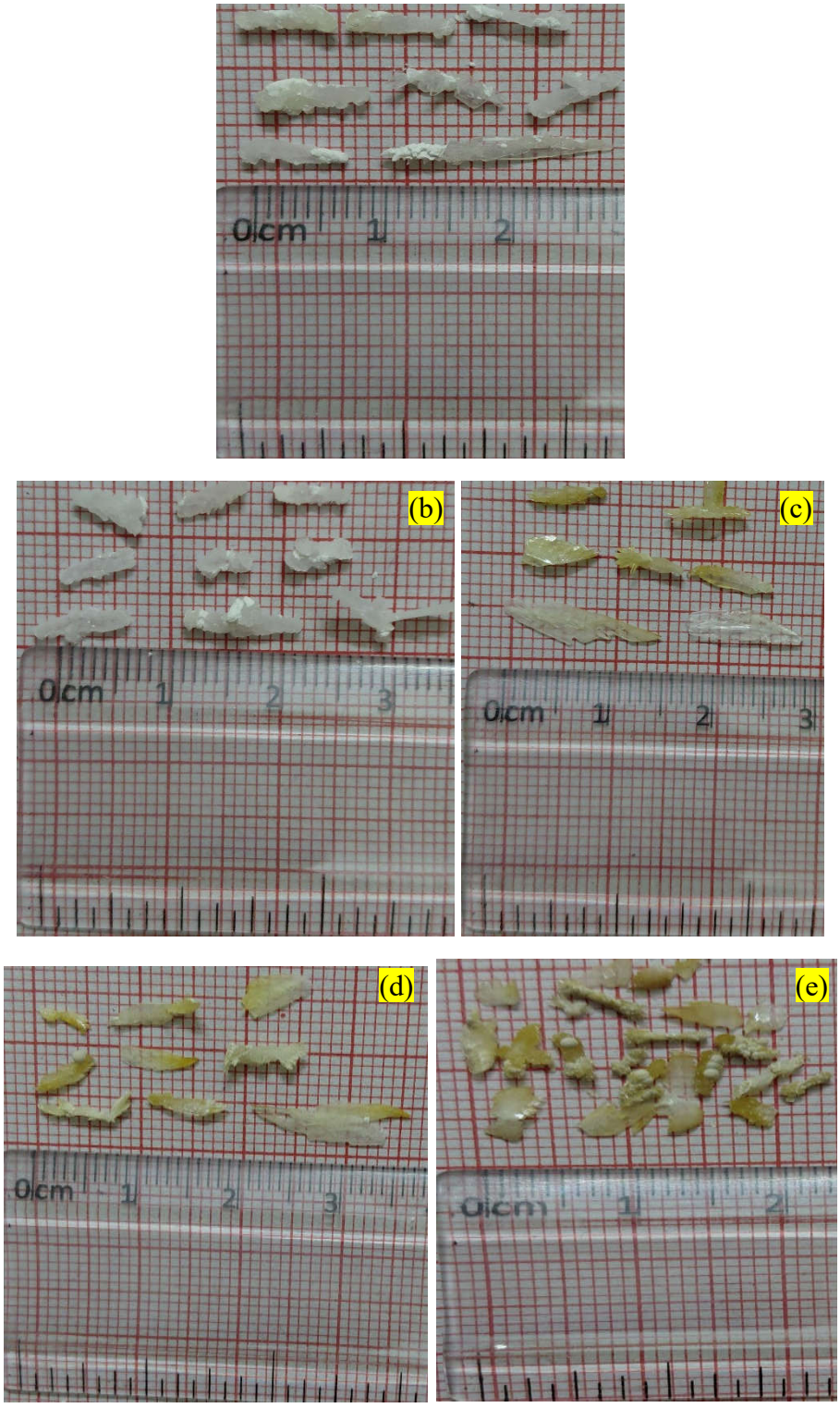

Fig. 8. Harvested Zn–CHPD crystals grown in the presence of different concentrations of Pedalium murex extract: (a) 0%, (b) 5%, (c) 10%, (d) 15% and (e) 20%.

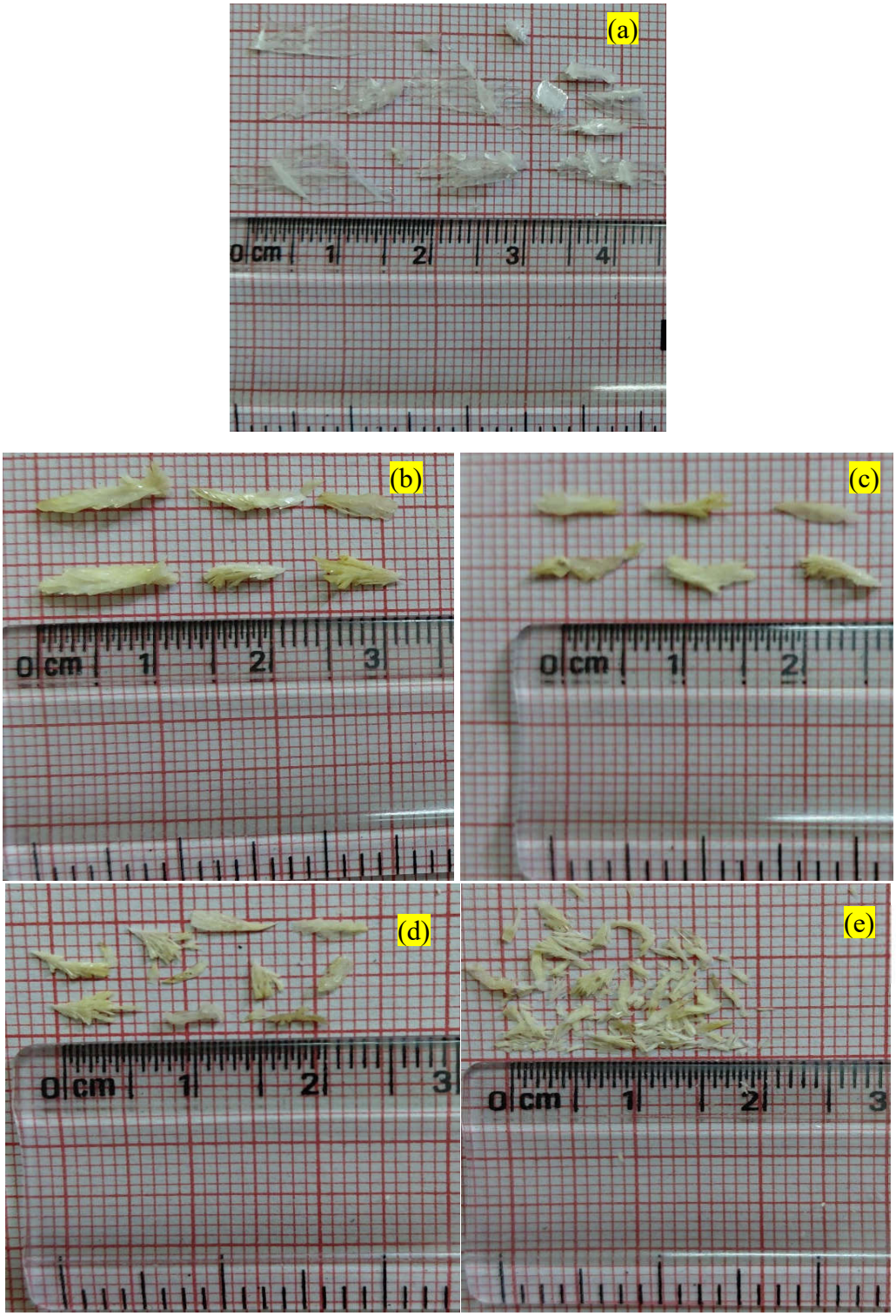

Fig. 9. Harvested CHPD crystals grown in the presence of different concentrations of Solanum xanthocarpum extract: (a) 0%, (b) 5%, (c) 10%, (d) 15% and (e) 20%.

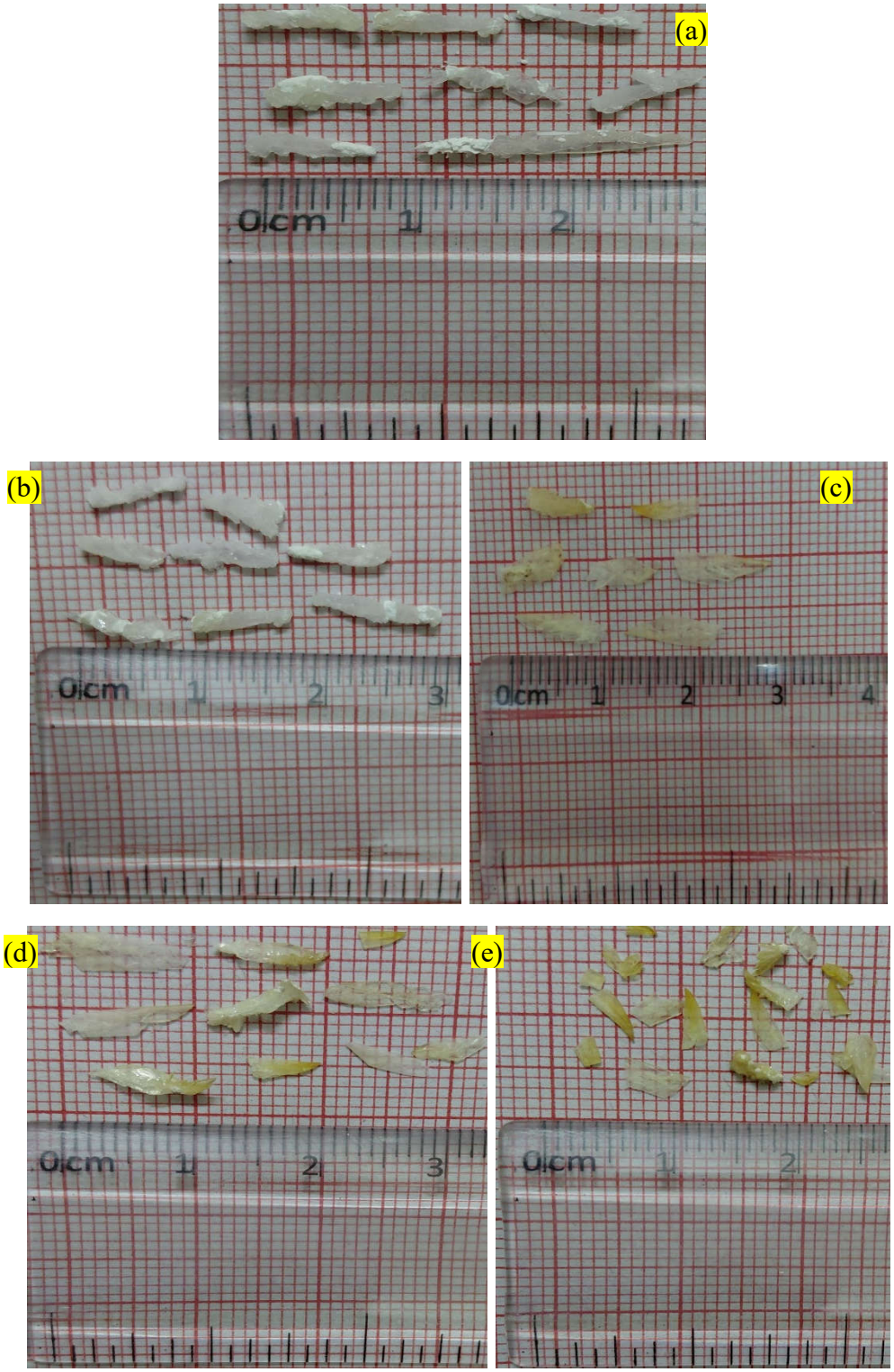

Fig. 10. Harvested Zn–CHPD crystals grown in the presence of different concentrations of Solanum xanthocarpum extract: (a) 0%, (b) 5%, (c) 10%, (d) 15% and (e) 20%.

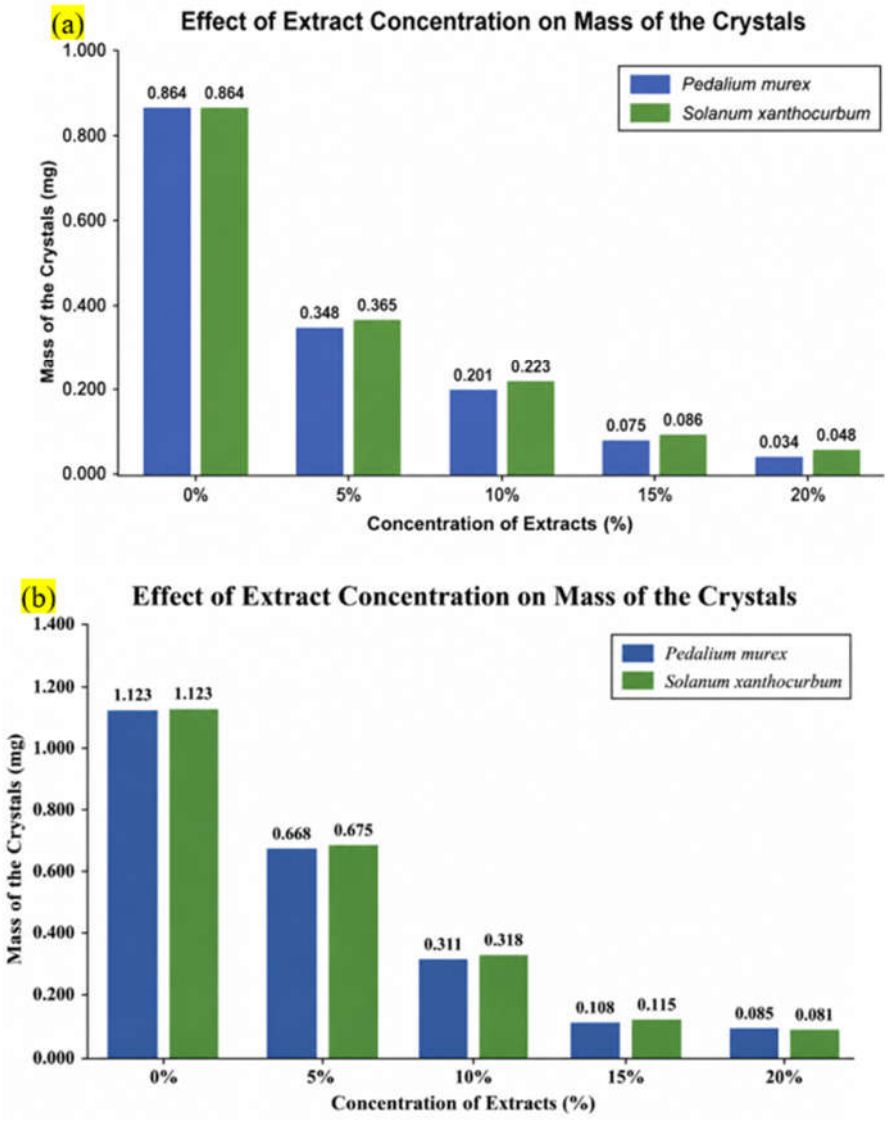

Figure 11 Mass (weight) of group (a) CHPD and (b) Zn – CHPD crystal by herbal extracts (*Pedalium murex, Solanum xanthocurbum*)

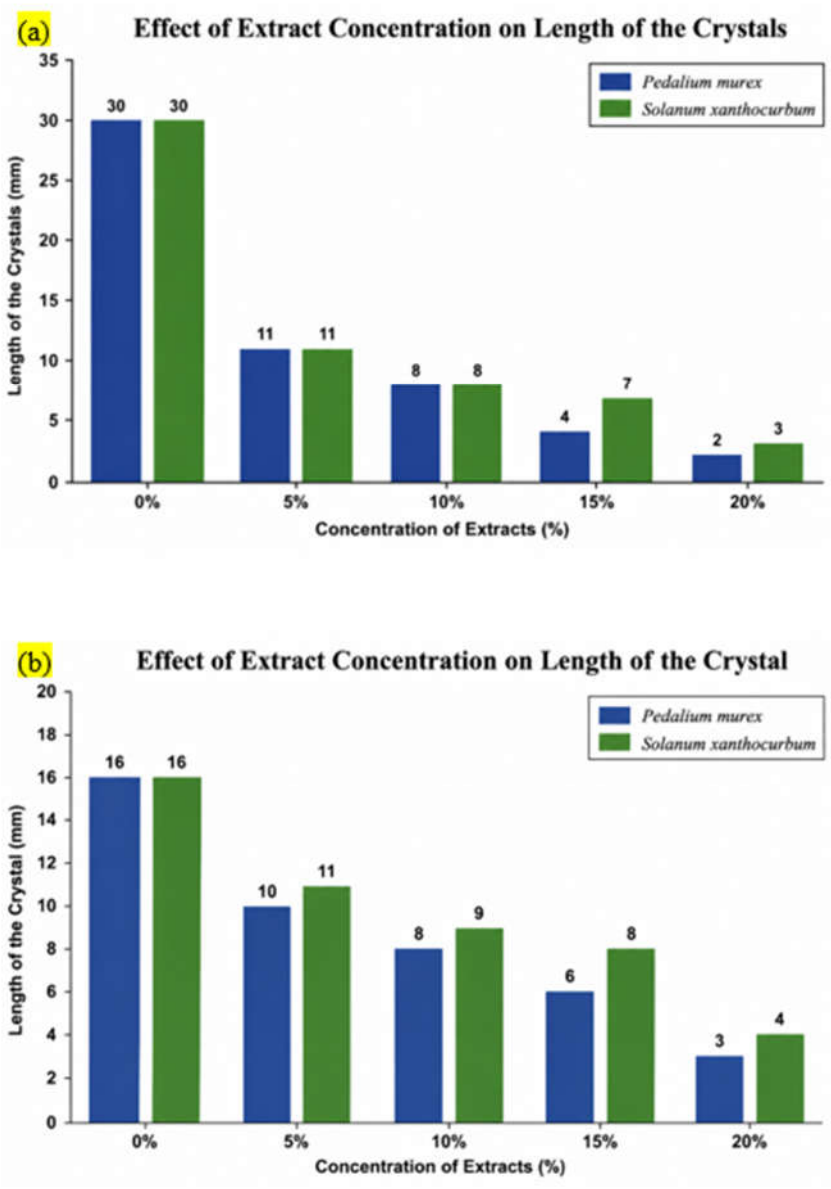

Figure 12 Length of group (a) CHPD and (b) Zn – CHPD crystal by herbal extracts (*Pedalium murex, Solanum xanthocurbu,*)